Desalination and Water Treatment
www.deswater.com

doi: 10.5004/dwt.2017.20736

75 (2017) 158–173
May

Removal of heavy metals from water by carbon nanocomposites prepared from melon wastes

Muneeb Ur Rahman[a], Muhammad Zahoor[b,*], Bakhtiar Ahmad[a]

[a]*Department of Chemistry, Hazara University, Mansehra, Pakistan, emails: muneeb_chem@yahoo.com (M. Ur Rahman), yousafzaibm@gmail.com (B. Ahmad)*
[b]*Department of Chemistry, University of Malakand, Chakdara, Dir (Lower), KPK, P.O. Box: 18000, Pakistan, email: mohammadzahoorus@yahoo.com*

Received 23 November 2016; Accepted 23 March 2017

ABSTRACT

In this study, a novel adsorbent was prepared from biomass and was characterized by surface area analyzer, Fourier transform infrared spectroscopy, X-ray diffraction, energy-dispersive X-ray spectroscopy, scanning electron microscope and thermogravimetric/differential thermal analyzer. The prepared nanocomposites were used for the removal of selected heavy metals from water. Freundlich and Langmuir isotherms were used to analyze the adsorption equilibrium data. The best fit was observed for Freundlich isotherm. The equilibrium time of adsorption of arsenic, chromium, copper, lead and zinc on the prepared adsorbent were 240, 260, 240, 220 and 180 min, respectively. With the increase in pH there was decline in percentage adsorption of the metals. The pseudo-first-order and pseudo-second-order kinetic models were applied to explain kinetics of adsorption. The best fit was obtained with second-order kinetic model. With increase in temperature there was an increase in the adsorption capacity which was evident from the positive values ΔS° and negative values of ΔH° and ΔG° (exothermic and spontaneous process).

Keywords: Melon wastes; Carbon nanocomposites; Adsorption; Intraparticle adsorption

1. Introduction

Clean and safe drinking water is important for humans and other living things for survival on earth, as water quality have effects on their health [1,2]. Groundwater is the major source of water supply for agricultural, industrial and domestic uses in almost all parts of the world. According to WHO, 80% of the diseases in the world are caused by inadequate sanitation, pollution and unavailability of clean water [3]. Drinking water pollution is a serious problem that has been resulted from unprecedented population growth, urbanization, and industrialization since 1990 [4,5]. Generally, drinking water contains different anions and heavy metals including Cd, Cr, Co, Hg, Ni, Pb, Zn, etc. These metals have significant adverse effects on human health that will be either through deficiency or toxicity due to excessive intake [2–5].

In the developing countries, most of the mortality and morbidity associated with water-related diseases are directly due to infectious agents and toxic substances like arsenic, fluoride, lead, manganese, chromium, copper, iron and zinc. Most of the heavy metal ions are toxic to living organisms [6]. They are not biodegradable and are persistent [7]. Therefore, the elimination of heavy metals from water and wastewater is important to protect public health [8]. Previous water treatment efforts had led to the development of various treatment technological options which involved the application of unit operations or unit processes such as chemical precipitation [9], coagulation [10], adsorption [11], ion exchange [12] and membrane filtration [13]. Furthermore, among aforementioned treatment technologies, adsorption had been reported as the most technically and economically viable option [14]. Research in water treatment by adsorption has resulted in development of different

* Corresponding author.

adsorbents from different materials such as activated carbon prepared from natural products, zeolites, aluminosilicate, peat kaolin, clay, nanomaterials and polysaccharides [15–25].

Although traditional sorbents could remove heavy metals from wastewater. However, the low sorption capacities and efficiencies limit their applications deeply. Among the traditional adsorbents activated carbon is the most efficient adsorbent that has high adsorption capacity due to its high surface area. However, the settling time of activated carbons is high due to its light weight which limits its use in water treatment processes. Magnetic adsorbents have been used as alternative by a number of authors but due to low surface area these adsorbents could not gained much importance. Thus, there is need for such adsorbents having comparable surface area as that of activated carbon on one hand and magnet properties on the other hand, thus they can be easily separated from solution after treatment through magnetic process [24].

Owing to the importance of adsorption process, the present study was aimed to prepare a novel adsorbent from melon wastes. The novel adsorbent was used for the removal of As, Cr, Cu, Pb and Zn from water.

2. Material and methods

2.1. Preparation and characterization of magnetic carbon nanocomposites

For the preparation of magnetic carbon nanocomposites the waste of melon were taken from local market. They were cut into pieces, then dried and transferred to $FeCl_3.6H_2O$ (10% w/v) solution in ethanol for 24 h. The biomass was then separated from the solution and dried in air at room temperature. The dried mass was then charred in a specially designed assembly, consists of a container, an inlet for nitrogen, an exhaust outlet for gases, electric heater and wire gauze (Fig. 1).

The prepared adsorbent was characterized by surface area analyzer, Fourier transform infrared spectroscopy (FTIR), X-ray diffraction (XRD), energy-dispersive X-ray spectroscopy (EDX), scanning electron microscope (SEM) and thermogravimetric/differential thermal analyzer (TG/DTA). For surface area analysis, a sample weighing of 0.1 g was taken and characterized by using surface area analyzer of model NOVA 2200e, Quantachrome, USA. The purging gas used was nitrogen.

The XRD analysis of the prepared adsorbent was carried out by using X-Ray Diffractometer (Joel, JDX-3532) having Ni-filter while monochromatic Cu Kα was used as a source of radiation which operates at a wavelength of 1.5518 Å. The X-ray generator was run at 45 kV and 30 mA. The speed and range for scanning was $2\theta/\theta$ and 10 min^{-1}, respectively.

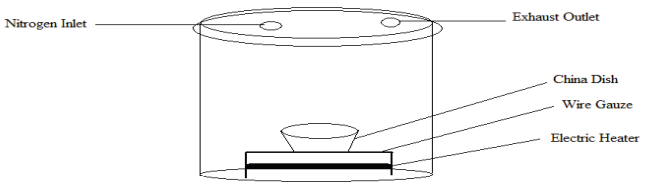

Fig. 1. The chamber used for preparation of magnetic carbon nanocomposites.

The FTIR spectra were taken by using FTIR spectrophotometer (IR Prestige-21, Shimadzu, Japan). The scanning range was set for mid-region as 700–500 cm^{-1} and for far region as 4,000–600 cm^{-1}.

Morphology of the sample was measured by placing the sample on the grid of SEM, whereas sputter coater was used for gold coating of the sample (made in USA). The images for surface morphology was then recorded by SEM with voltage of 20 kV (Joel, JSM-5910).

The prepared adsorbents were analyzed by TG/DTA of diamond series made in USA having a reference of aluminum trioxide as a standard. The EDX analysis was performed using EDX model INCA 200.

2.2. Kinetic parameters determination

A series of 25 mL flasks were taken and were spiked with known amount of heavy metal to achieve a concentration of 200 ppm. A concentration of 0.5% (w/v) of the prepared adsorbent was then added in each flask and arbitrary rotated with a speed of 300 rpm at a temperature of 25°C. Every flask was then subjected to a magnetic bar for the separation of sorbent. Finally, the solutions were filtered through Whatman No. 1 filter paper and were subjected to atomic absorption analysis.

2.3. Adsorption parameters determination

Different concentration solutions (150, 175, 200, 225, 250, 275, 300, 325 and 350 ppm) of the heavy metals were prepared in 25 mL flasks and to each flask 0.5% (w/v) of the prepared adsorbent was added. These flasks were then shaken on orbital shaker at 300 rpm for 480 min at room temperature followed by the atomic absorption analysis.

2.4. Determination of effect of pH on adsorption of heavy metals

A series of solutions having same concentration (200 ppm) of the heavy metals were taken in 25 mL flasks. The pH of the solutions in flasks was adjusted ranging from 1 to 14 by adding NaOH or HCl. Each flask was spiked with prepared adsorbent in a ratio mentioned above and were shaken at 300 rpm for 480 min on orbital shaker. Thereafter the sorbents were removed by using magnetic bar and were subjected to atomic absorption analysis.

2.5. Thermodynamics parameters determination

A series of flasks containing 200 ppm solutions of the selected heavy metals were spiked with adsorbent. The flasks were kept at various temperatures while shaking on orbital shaker for abovementioned period. The adsorbent was then separated from solutions and were subjected to atomic adsorption analysis.

3. Results and discussion

3.1. Characterization of Fe_2O_3 magnetic carbon nanocomposites made from melon wastes

A specially designed chamber as shown in Fig. 1 was used to prepare magnetic adsorbent from melon waste (peel). The

magnetic properties of the prepared adsorbent were noted by subjecting it to the magnetic bar. The attraction of the adsorbent toward magnet bar confirmed the magnetic character of the prepared adsorbent.

Figs. 2 and 3 show the surface area and pore distribution of magnetic adsorbent, respectively, whereas Table 1 shows different surface parameters of the prepared adsorbent.

The XRD spectra of the prepared adsorbent are shown in Fig. 4 suggesting that Fe_3O_4 has been deposited on graphitic surface of the adsorbent. XRD is not only used for structural elucidation but also for particles size measurement [22]. The diffraction peaks at 2θ (28.45°, 31.71°, 35.65°, 43.65°, 55.1° and 58.9°) corresponding to indices 220, 311, 400, 422, 511 and 440 represents the cubic unit cells of the magnetite structure reported by Sundarajan and Ramalakshmi [22] and Kahani et al. [26]. The diffraction peaks at 2θ (11.28°, 12.75°, 16.6°, 22.75°, 40.65° and 50.35°) were related to goethite, maghemite and hematite as impurities [26]. The size of the prepared magnetic iron oxide and magnetic carbon nanocomposites were measured by using Debye–Scherer's Eq. (1) and were found to be in the range of 80–300 nm.

$$D = k\lambda/\beta\text{Cos}\theta \quad (1)$$

where D represents the mean size, k (0.94) is constant, λ (1.55060 Å) is the wavelength of X-ray, β shows excess line broadening while θ represents the Bragg angle. The value of β can be calculated from the following relation:

$$\beta = B - b \quad (2)$$

where B is the line width (in radian) and b shows instruments line broadening (in radian) [26]. For the characterization of

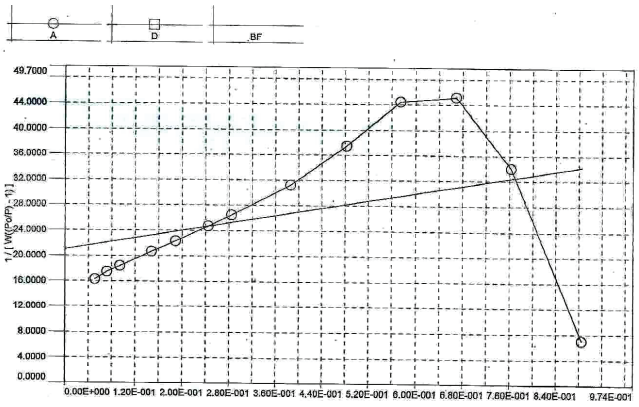

Fig. 2. Graph showing BET surface area of the synthesized iron oxide magnetic and magnetic carbon nanocomposites from melon waste.

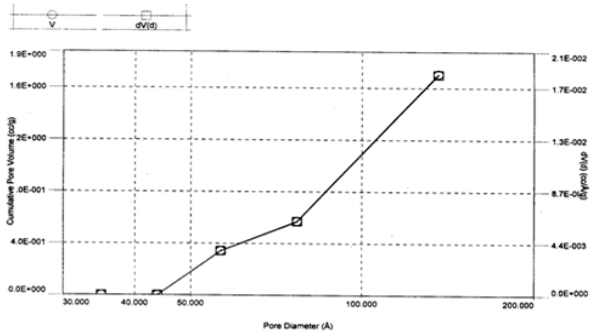

Fig. 3. Graphical repsentation of pores distribution in the prepared adsorbent from melon waste.

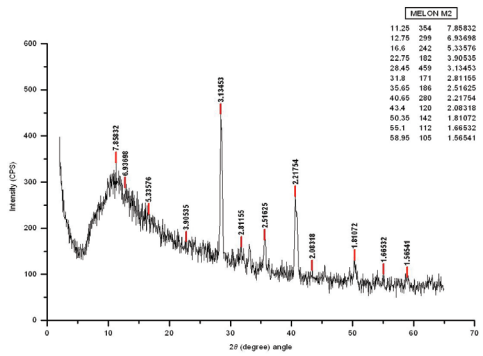

Fig. 4. XRD pattern of magnetic carbon nanocomposites prepared from melon waste.

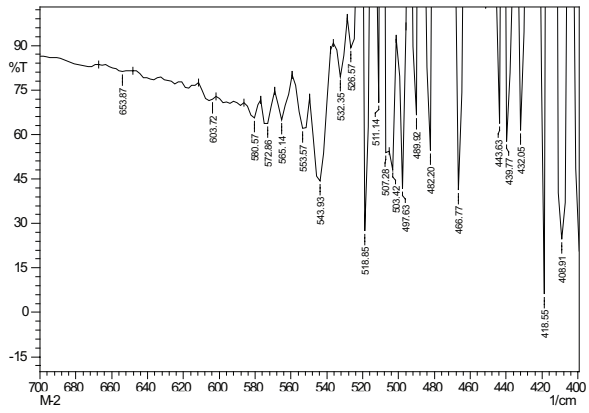

Fig. 5. Far IR spectra of magnetic carbon nanocomposites prepared from melon waste.

Table 1
Physical parameters of the activated carbon and carbon nanocomposites prepared from melon waste

Material	BET, surface area ($m^2\ g^{-1}$)	Langmuir, surface area ($m^2\ g^{-1}$)	Pores volume, total ($cm^3\ g^{-1}$)	Micropores volume ($cm^3\ g^{-1}$)	Pore diameter, average (Å)
Powdered activated carbon	136.45	840.34	3.54	0.97	154.8
Carbon nanocomposites	100.77	567.21	2.07	0.81	154.39

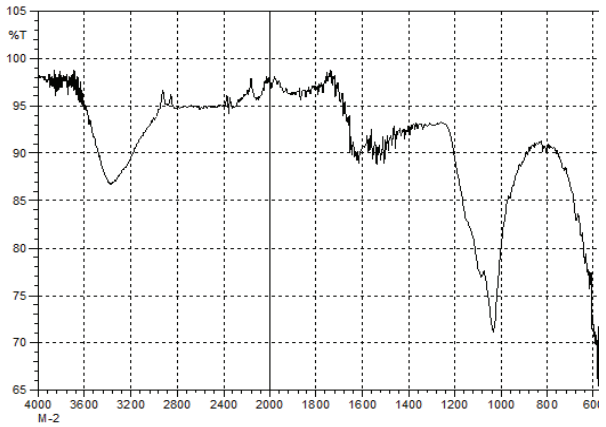

Fig. 6. Mid-IR spectra of magnetic carbon nanocomposites prepared from melon waste.

the nanocomposites the most widely used technique is the IR spectroscopy. The FTIR spectra show the nature of surface functional groups. The IR spectra of the prepared adsorbent showed the broad band in the range of 1,000–1,200 cm^{-1} which were attributed to stretching of C–C and C–O whereas peak at 596.65 cm^{-1} was attributed to the stretching of Fe–O (magnetite). The same pattern has been observed by Kahani et al. [26] (Figs. 5 and 6).

Fig. 7 represents the morphology of the adsorbent. The SEM images showing variation of sizes and shapes of the nanocomposites where white patches shows iron oxide in crystalline form and the black spots are related to the carbon. The aggregation of the iron oxide is attributed to moisture content adsorbed by the prepared adsorbent. The images showed the spherical shape of iron oxide and the sizes of nanocomposites depicted were in the range of 70–300 nm.

Fig. 8 shows the TG/DTA spectra of nanocomposite. The loss of mass takes place at two points. A 28.3% mass loss

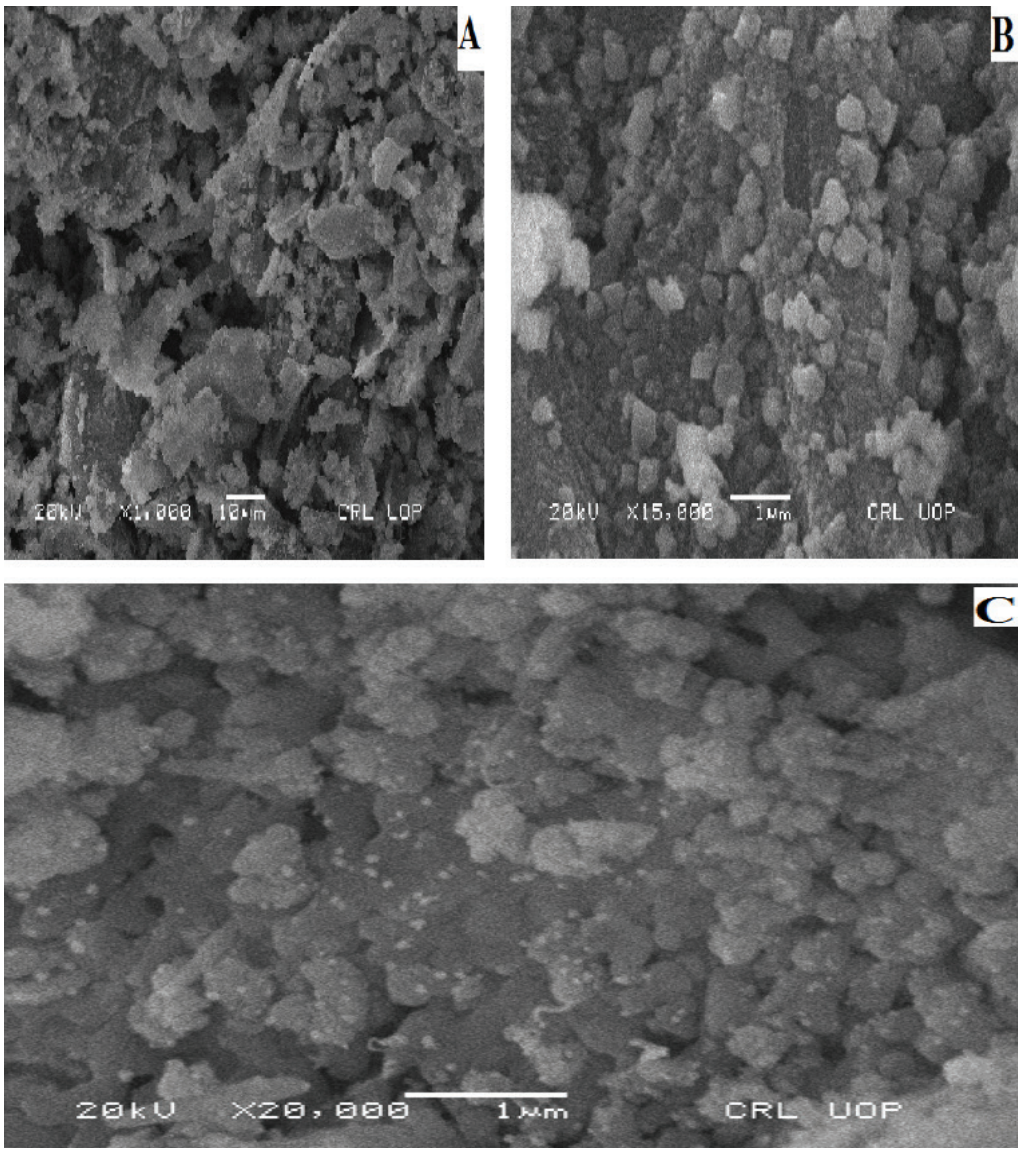

Fig. 7. SEM images of magnetic carbon nanocomposites prepared from melon waste at different magnification.

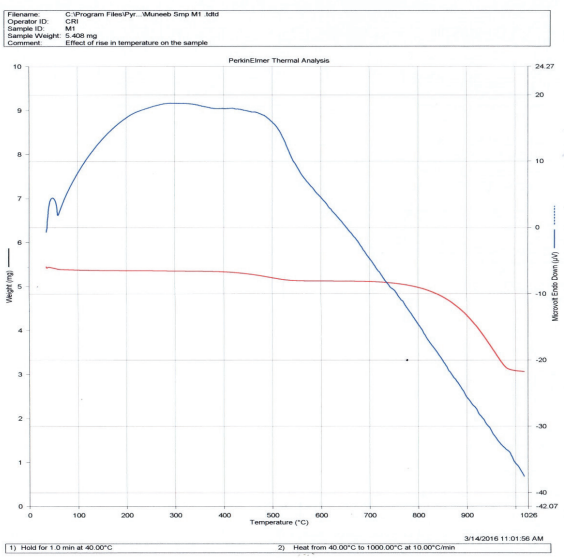

Fig. 8. TG/DTA curves of magnetic carbon nanocomposites prepared from melon waste.

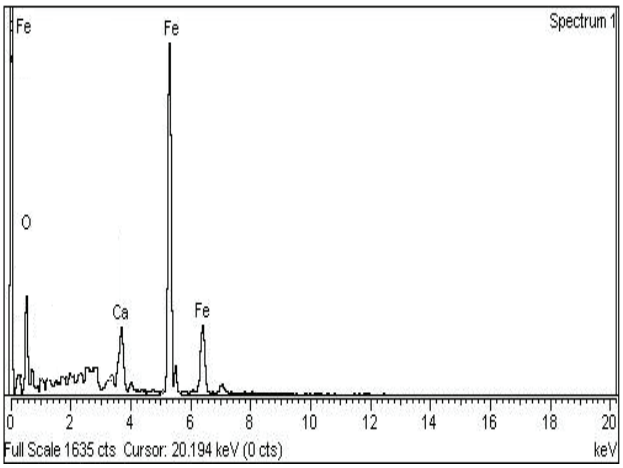

Fig. 9. EDX spectra of magnetic carbon nanocomposites prepared from melon waste.

was noted at temperature ranging from 400°C to 820°C with endothermic peak whereas further loss of mass of about 47.6% was noted in the range of 820°C–980°C.

Fig. 9 shows the EDX spectra of the prepared adsorbent. The spectra reveal the existence of carbon, ferrous and oxygen. Whereas a small peak of calcium as impurity is also present. As already reported by Kahani et al. [26] that Fe-Lα, Fe-Kα O-Kα and Fe-Kβ are related to magnetite deposition in the composite [26].

3.2. Adsorption isotherm

3.2.1. Giles isotherms

The adsorption of heavy metal on the adsorbents prepared from melon waste was studied using Giles isotherm [27]. The classifications of Giles isotherms is based on initial slope of the curvature and are constant partition (*C*), the high affinity (*H*), the Langmuir (*L*) and sigmoidal (*S*) types.

The Giles adsorption isotherm of arsenic on adsorbent prepared from melon waste is given in Fig. 10. The isotherm in the figure is L type while for chromium, copper, zinc and lead it was C type.

3.2.2. Langmuir isotherm

Langmuir adsorption isotherm [28] assumes that the maximum adsorption corresponds to a saturated monolayer of solute molecules on the adsorbent surface, having no interaction with molecules adsorbed from lateral sides. The linear form of Langmuir isotherm is given as:

$$\frac{C}{q} = \frac{C}{Q_0} + \frac{1}{Q_0 b} \tag{3}$$

The above equation shows that q represents quantity of adsorbate adsorbed in mg g^{-1}, C represents the equilibrium concentration of adsorbate in mg L^{-1} while Q_0 and b are Langmuir constants. Q_0 is the maximum adsorption capacity of the adsorbent whereas b is the energy of the process.

Langmuir plot of specific adsorption (C/q) against equilibrium concentration (C) for the selected metals adsorption on the prepared nanocomposites is shown in Fig. 11.

The slope and intercept were used to calculate the values of Langmuir constants Q_0 and b. Their values are given in Table 2. The adsorption capacity of this adsorbent was comparable with those reported in references [23–25].

3.2.3. Freundlich isotherm

This isotherm is mostly used to explain the heterogeneous systems [29] and is given by the equation:

$$\ln q = \ln k + \frac{1}{n}\ln C \tag{4}$$

In the above equation, C shows the equilibrium concentration in mg L^{-1}, q is the amount of adsorbate adsorbed in mg g^{-1}, k and n are Freundlich constants. k shows adsorption capacity while n is the adsorption intensity. The Freundlich constants k and $1/n$ can be obtained from the slope and the intercept of the ln$C$ against ln$q$ plot.

For adsorption of heavy metals on adsorbent prepared from melon waste the Freundlich isotherms are given in Fig. 12.

From the R^2 values of Freundlich and Langmuir isotherms it was found that the data were fitted better by Freundlich isotherm rather than Langmuir isotherm (Table 2).

3.3. Adsorption kinetics

3.3.1. Effect of contact time

In adsorption processes contact time required for reaching equilibrium for an adsorbent is an important factor. For heavy metals the contact time required to reach equilibrium is shown in Fig. 13. In the first few minutes the uptake of arsenic was very fast as initially more sites of adsorbent were available for adsorption of metal. As the time passes maximum number of sites are occupied by the metals

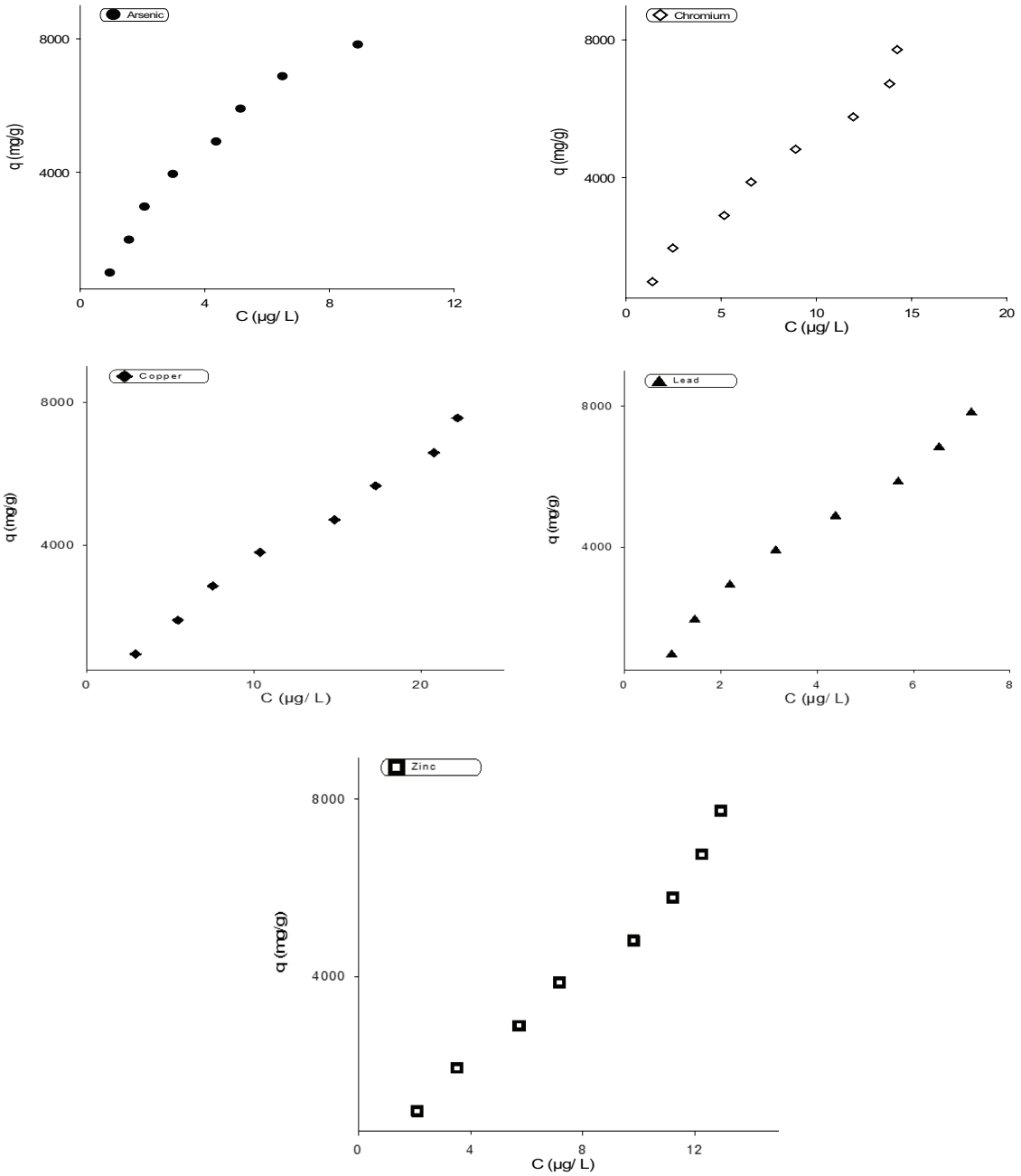

Fig. 10. Plot for Giles adsorption isotherm of selected heavy metals on nanocomposites of melon waste.

which slows down the adsorption process and equilibrium is reached. As shown in Fig. 13, the equilibrium time is 240, 260, 240, 220 and 180 min, respectively, for arsenic, chromium, copper, lead and zinc adsorption on adsorbent prepared from melon waste.

3.3.2. Adsorption kinetic models

The knowledge of adsorption kinetics plays a significant role in the removal of pollutants from water. The Lagergren first-order and pseudo-second-order [30,31] models were used for the determination of kinetic parameters.

3.3.2.1. Pseudo-first-order kinetics

The pseudo-first-order equation can be expressed by the relation:

$$\ln\left(q_e - q\right) = \ln q_e - k_a t \tag{5}$$

where q_e and q (mg g^{-1}) are the amount of adsorbate adsorbed at equilibrium and time t, respectively, and k_a (min^{-1}) is the rate constant. k_a can be calculated from slope of the plot of $\ln(q_e - q)$ vs. t (Fig. 14). The k_a and R^2 values are given in Table 3.

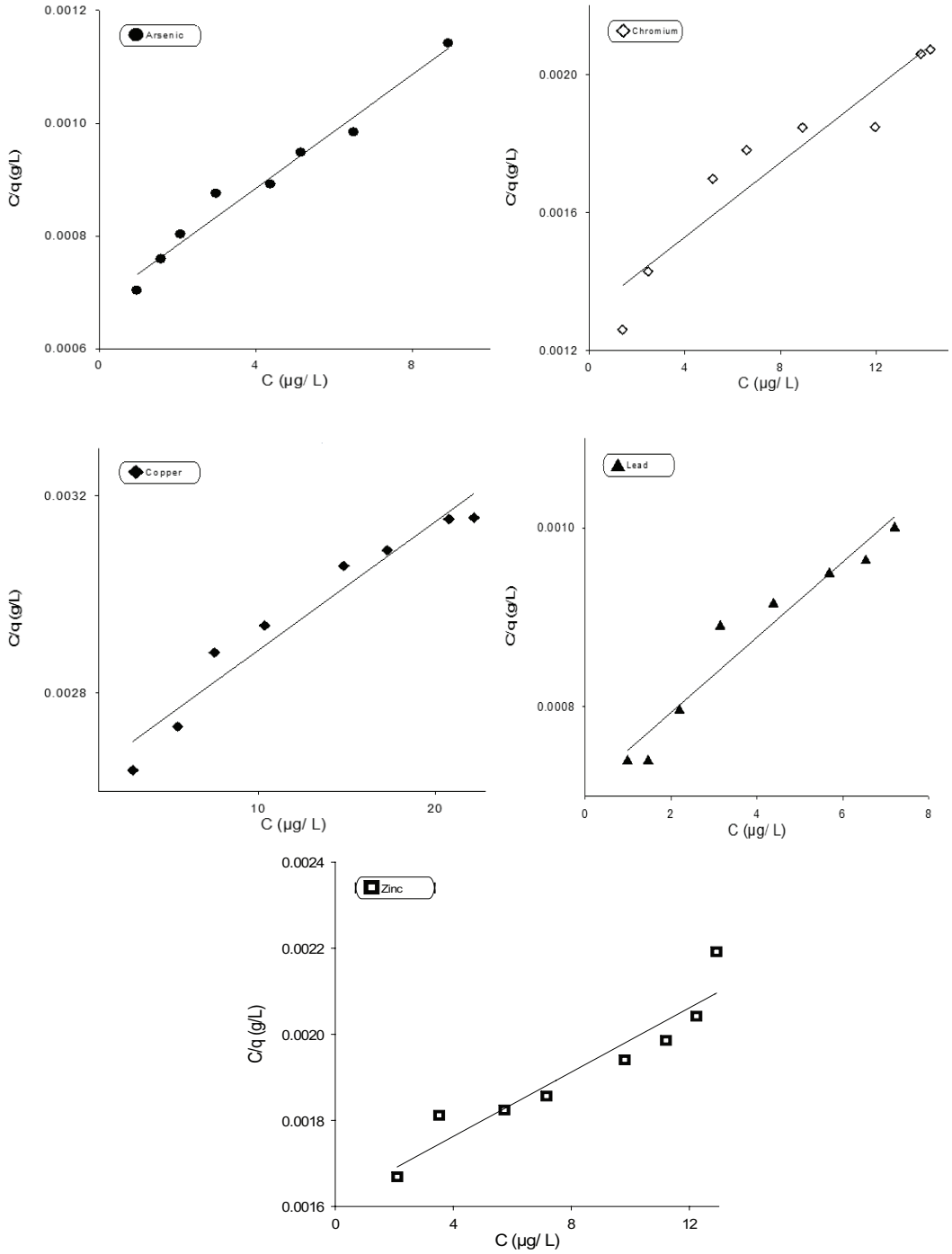

Fig. 11. Langmuir plot for the adsorption of heavy metals on adsorbent prepared from melon wastes.

3.3.2.2. Pseudo-second-order kinetics

The pseudo-second-order equation can be expressed by the relation:

$$\frac{t}{q_t} = \frac{1}{k_2 q^2} + \left(\frac{1}{q}\right)t \tag{6}$$

where k_2 (g mg^{-1} min^{-1}) is the rate constant of adsorption, q (mg g^{-1}) is the amount of adsorbate adsorbed at equilibrium and q_t at time t. The values of k_2 and q were calculated from intercept and slope of the straight line, respectively.

The k_a and R^2 values are given in Table 3 and were calculated from t/q_t vs. t plots of heavy metals adsorption on adsorbent prepared from melon waste (Fig. 15).

Table 2
Langmuir adsorption constants for heavy metals on nanostructures from melon waste

Heavy metals	Langmuir constant		R^2	Freundlich constant		R^2
	Q_0	b		$1/n$	k	
Arsenic	19,841	0.074	0.972411	0.9257	1,231.82	0.95194
Chromium	18,484	0.041	0.9014	0.8192	806.722	0.9867
Copper	38,285	0.0099	0.9431	0.9784	356.49	0.9915
Lead	23,752	0.0593	0.9386	0.9568	1,203.40	0.9694
Zinc	26,798	0.0231	0.8935	1.0752	452.73	0.9907

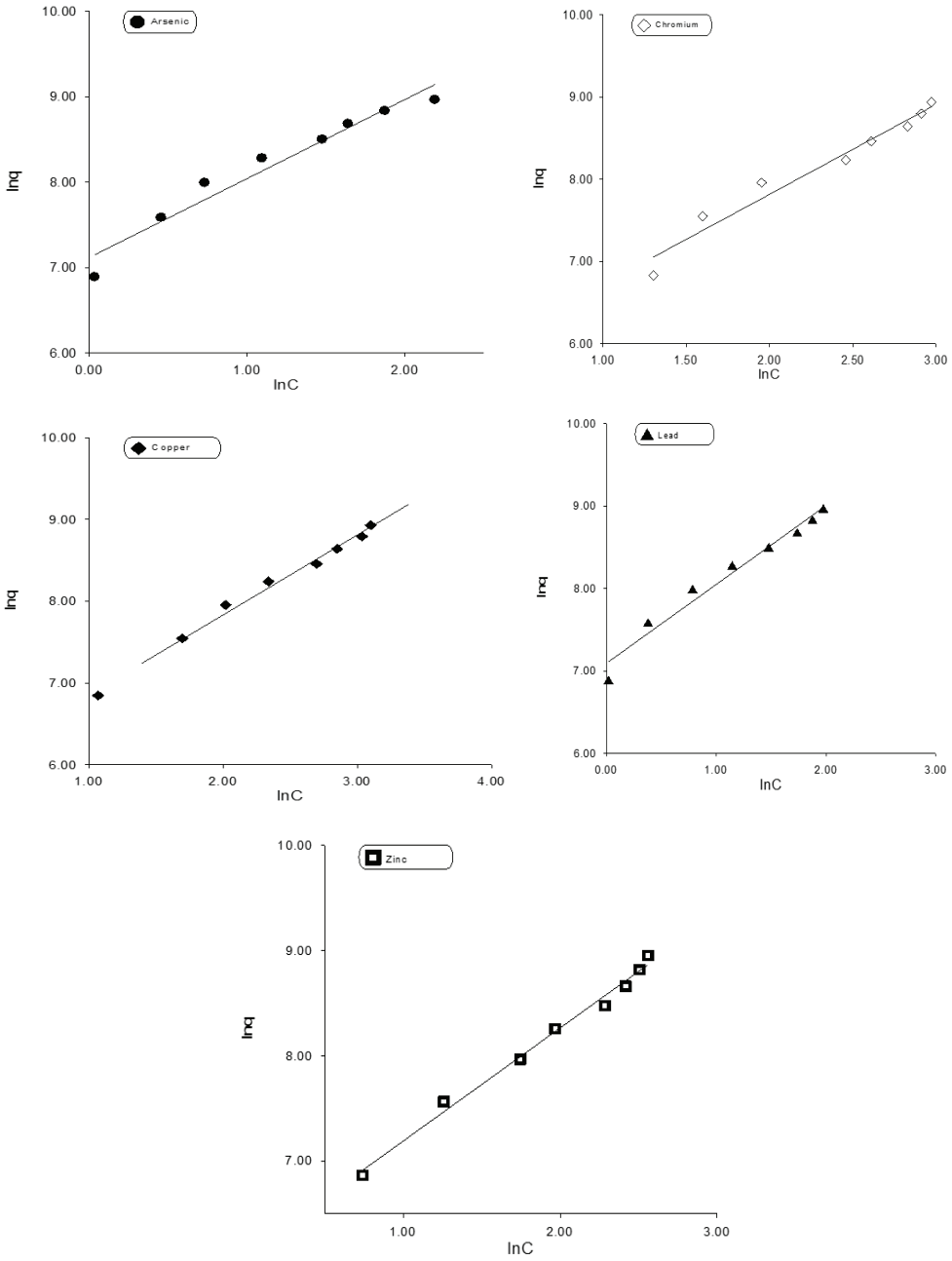

Fig. 12. Freundlich plot for the adsorption of heavy metals on adsorbent prepared from melon wastes.

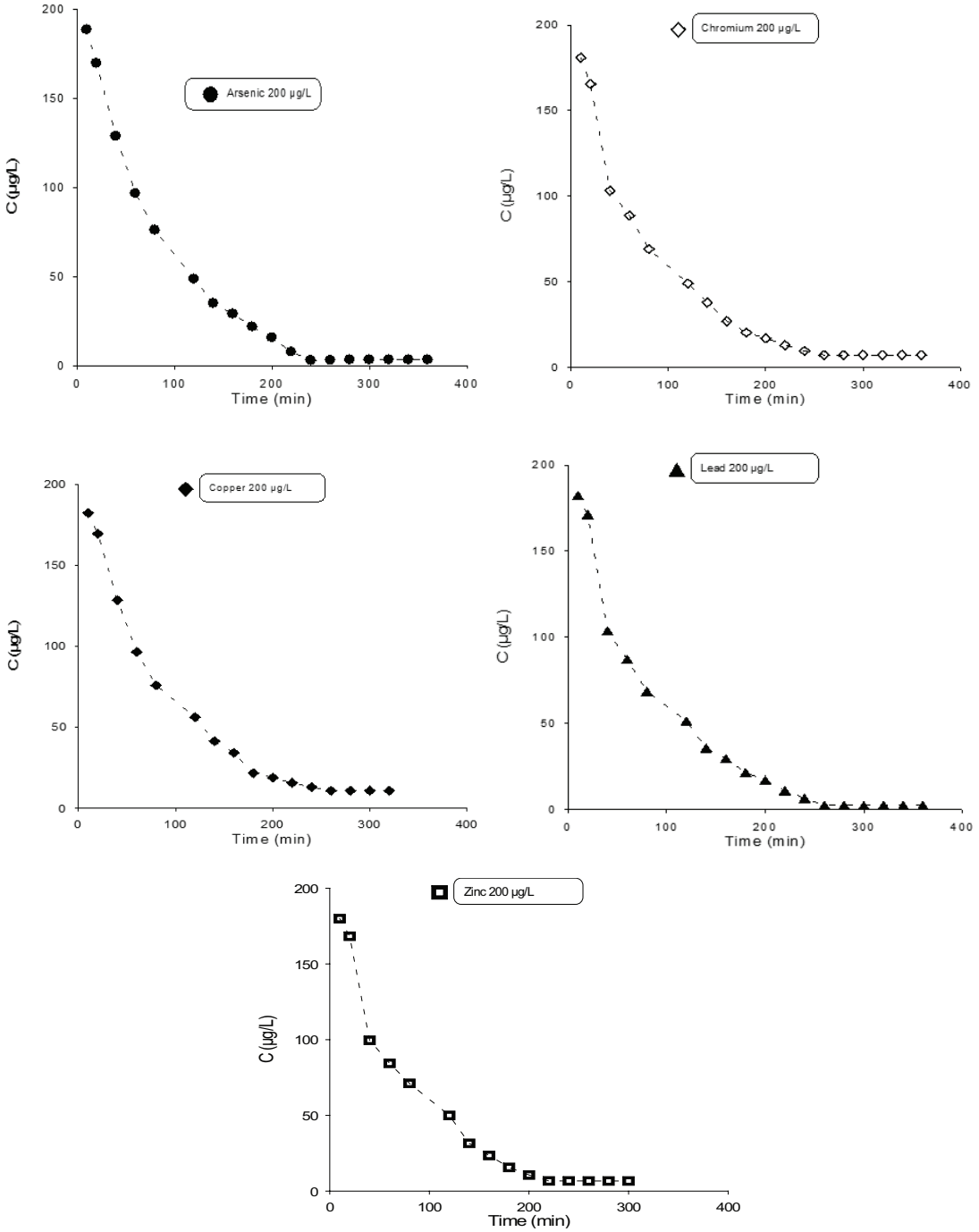

Fig. 13. The plot for effect of contact time for adsorption of metals on nanocomposites of melon waste.

Table 3 shows that the adsorption kinetics could be best explained in terms of the pseudo-second-order rate equation with precision in the correlation coefficients as compared with pseudo-first-order rate equation.

3.4. Adsorption mechanism

In the adsorption process the main steps involved in the removal of adsorbate by adsorbent are:

- Transport of ingoing particles to the external surface of the adsorbent.
- Transport of the adsorbate through the pores of adsorbent except for a small amount of the adsorption which occurs on the external surface (intraparticle diffusion) and adsorption of the ingoing particles (adsorbate) on to interior surface of the adsorbent.
- Among them the rate controlling step affects the overall adsorption process.

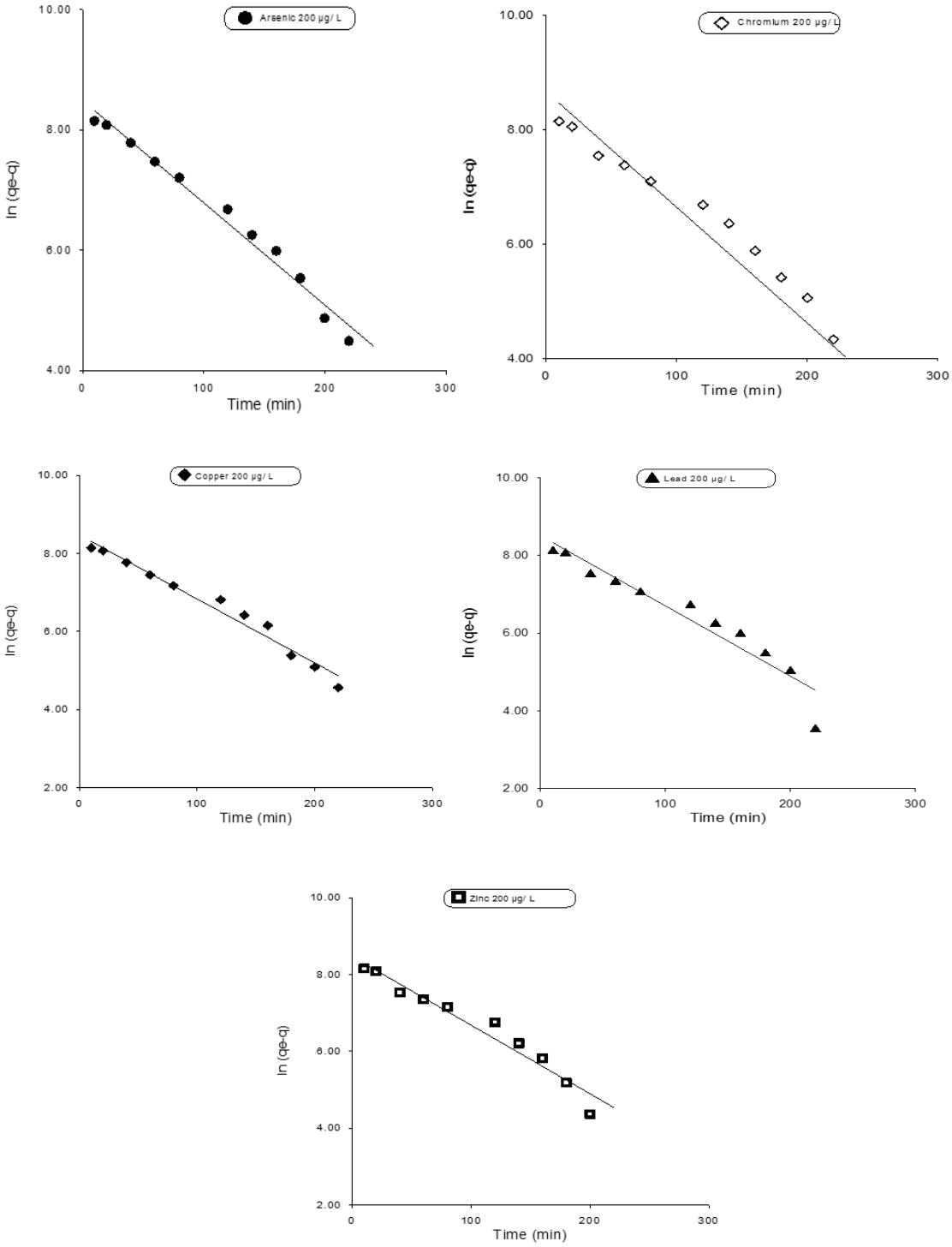

Fig. 14. Pseudo-first-order kinetic plots for the adsorption of metals on magnetic carbon nanocomposites prepared from melon waste.

3.4.1. Effect of intraparticle diffusion

For the determination of the rate controlling step, the kinetic results were fitted to the intraparticle diffusion model of Weber's [32]:

$$q_{t=}k_{id}t_{\frac{1}{2}}+C \quad (7)$$

where C is the intercept, k_{id} (mg g^{-1} min$^{-0.5}$) indicates intraparticle diffusion rate constant, which can be evaluated from slope q_t vs. $t^{1/2}$ plot. If the regression of q_t vs. $t^{1/2}$ is linear and passes through the origin, the only rate-limiting step will be intraparticle diffusion.

For the understanding of kinetic mechanism, the amount of metals adsorbed on the graphitic magnetic carbon

Table 3
Rate constants and correlation coefficients of pseudo-first-order and pseudo-second-order kinetic models of heavy metals adsorption on graphitic magnetic carbon nanostructures

Heavy metal	Pseudo-first-order kinetic model		Pseudo-second-order kinetic model	
	k_a	R^2	k_2	R^2
Arsenic	0.0170291	0.982313	1.37×10^{-6}	0.972
Chromium	0.0202407	0.888353	2.36×10^{-6}	0.987
Copper	0.017603	0.964158	1.44×10^{-6}	0.984
Lead	0.0180598	0.920853	1.96×10^{-6}	0.988
Zinc	0.0178322	0.952611	1.57×10^{-6}	0.987

nanostructures prepared from melon waste, was plotted vs. the square root of time (Fig. 16). Figures showed an initial curve followed by the linear relationship. The initial curve can be explained by the boundary layer effect while the linear part corresponds to the intraparticle diffusion.

The linear plots deviate from the origin clearly indicating that the adsorption of these metals have more than one controlling steps.

3.5. Effect of pH

One of the most important factors that affects the adsorption process is pH because it affects surface charge of the prepared adsorbent, degree of ionization and speciation of the adsorbate.

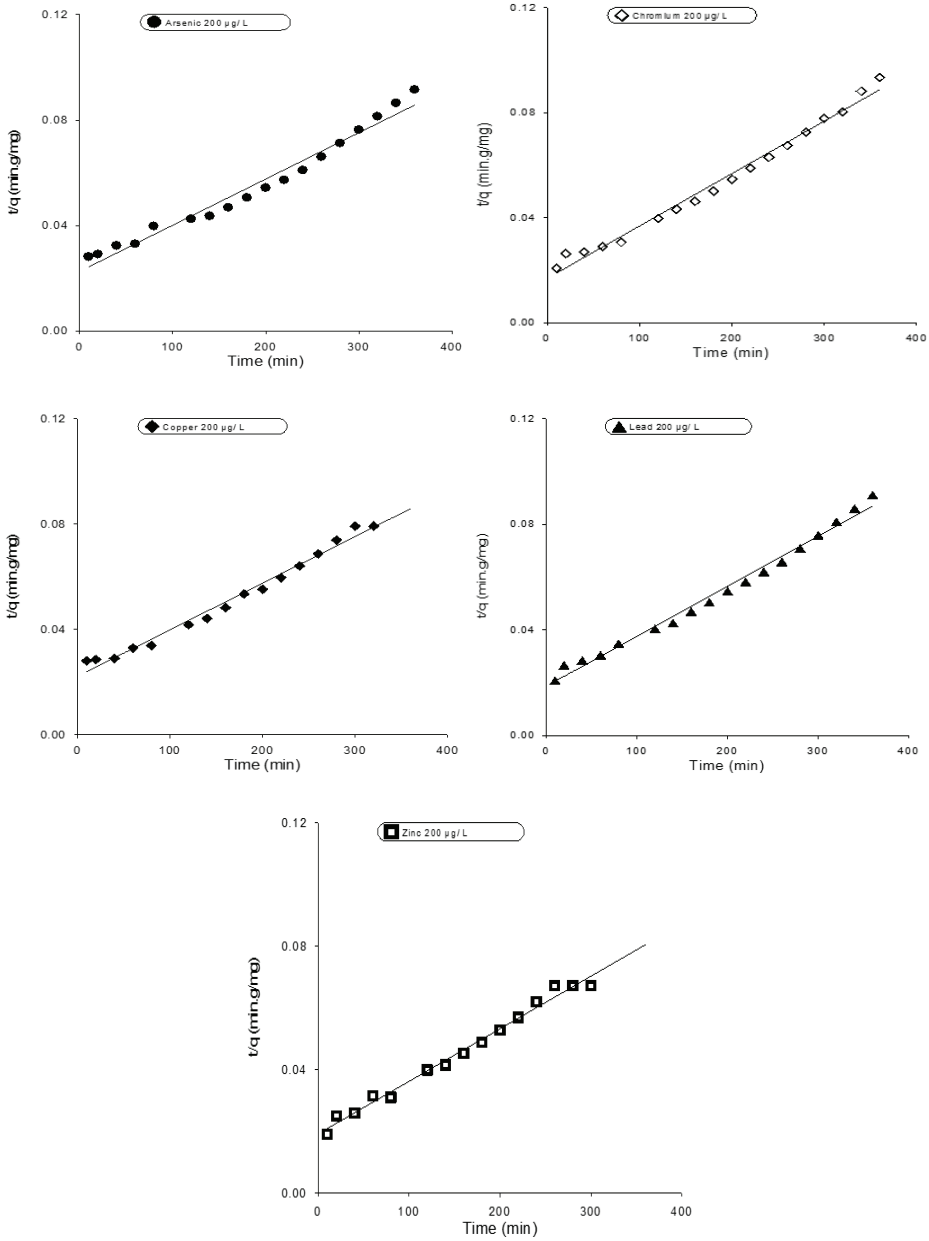

Fig. 15. Pseudo-second-order kinetic plots for the adsorption of arsenic on magnetic carbon nanocomposites prepared from melon waste.

The effect of pH on adsorption of metals is shown in Fig. 17. The figures indicate that the adsorption of arsenic at pH from 1 to 9 was not affected; however, a decline was noted above pH 9. For chromium, the adsorption from 1 to 7 pH was not affected; however, a decline was noted at above pH 7 while for copper adsorption there was gradual decrease in percentage adsorption with rise in pH. The adsorption of lead was not affected in the pH range 1–10 and above this range a decline was observed. There was no effect of pH on zinc adsorption from 1 to 8 above which a decline was notable.

3.6. Adsorption thermodynamics

To determine the adsorption thermodynamics, adsorption experiments were carried out at 30°C, 40°C, 50°C and 60°C. The Van't Hoff equation was used to determine the values of $\Delta H°$ and $\Delta S°$ of the adsorption process:

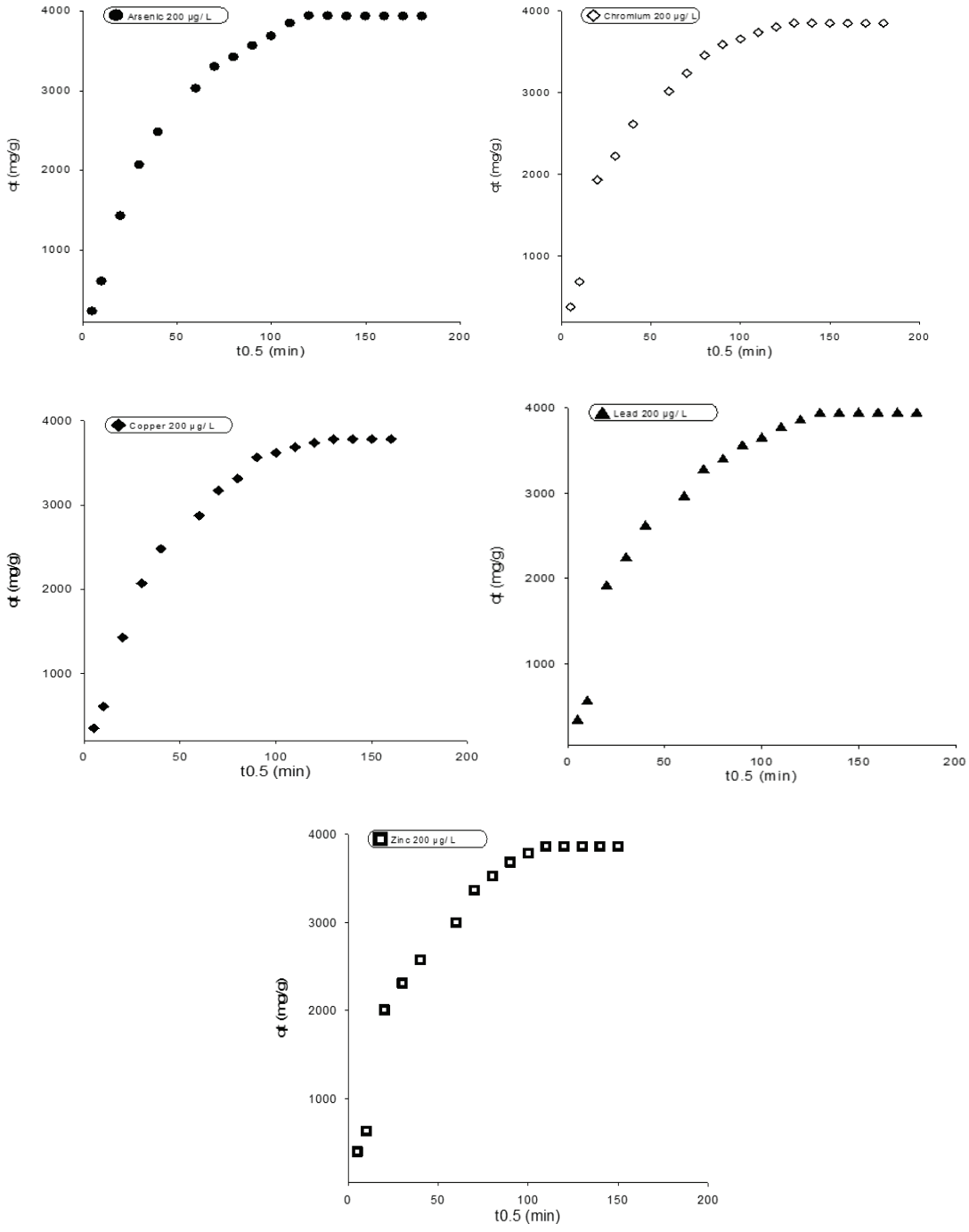

Fig. 16. The intraparticle diffusion plot for the adsorption of heavy metals on iron oxide carbon nanocomposite prepared from melon waste.

$$\ln k = \frac{\Delta S^\circ}{R} - \frac{\Delta H}{RT} \quad (8)$$

where k is the distribution constant of adsorption, ΔH° is the enthalpy change and ΔS° is the entropy change, T is temperature in Kelvin while R is universal gas constant.

The value of ΔH° was calculated from the slope while ΔS° was calculated from intercept of the ln$K$ and $1/T$ plot (Fig. 18) for adsorption of arsenic on adsorbent prepared from melon wastes. The values of ΔH° and ΔS° are given in Table 4.

The positive value of ΔS° from Table 4, indicated that during the adsorption process, there is an increase, in the randomness solid/solution system interface whereas the negative values of ΔH° showed that the selected metals adsorption on the prepared iron oxide and magnetic carbon nanocomposites, is an exothermic process.

The values of standard free energy ΔG° were calculated from Eq. (9) and are given in Table 5.

$$\Delta G^\circ = \Delta H^\circ - T\Delta S^\circ \quad (9)$$

The spontaneous character of the process is evident from the negative values of ΔG° at different temperatures. With increase in temperature the value of ΔG° also increases which shows that at high temperature the adsorption process is more favorable. It was concluded that the adsorbent

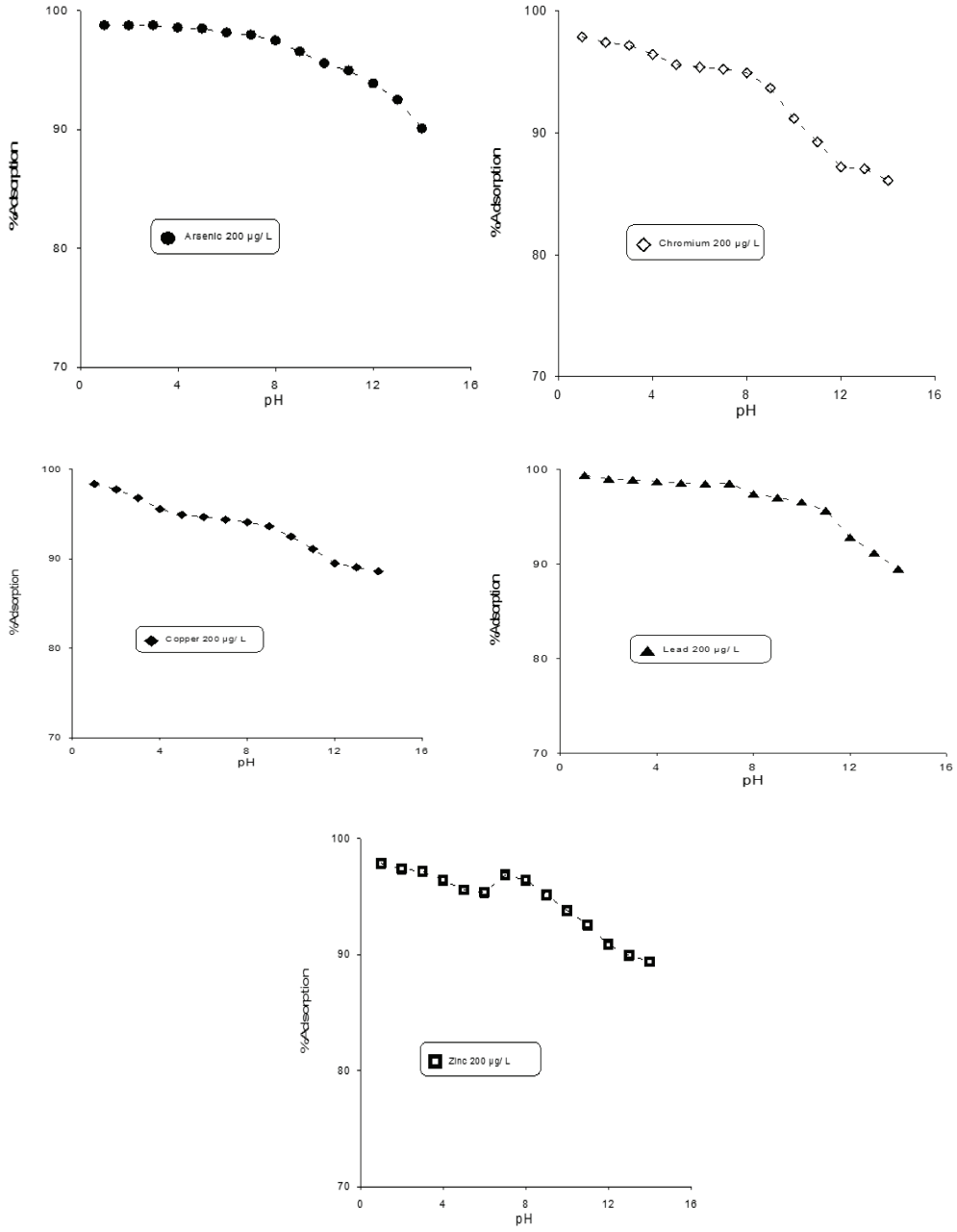

Fig. 17. Effect of pH on metals adsorption on magnetic carbon nanocomposites prepared from melon waste.

prepared from the biomass can be used as alternative of the activated carbon for the removal of heavy metals from water.

3.7. Regeneration of the adsorbent

From environmental and economic point of view the regeneration of the adsorbent is very important as any adsorbent that cannot be regenerated may lead to secondary environmental problem and loss of economy. For the regeneration the metal laden adsorbent, it was treated with various concentration solutions of hydrochloric acid ranging from 0.01 to 0.2 N. The percentage removal of the metals increased with increase in acid concentration in the medium. Maximum regeneration was achieved at 0.1 N HCl solutions for the selected metals laden adsorbents (Fig. 19).

4. Conclusions

A novel biosorbent was prepared from peel of melon which was then characterized by surface area analyzer, FTIR, XRD, EDX, SEM and TG/DTA. Freundlich and Langmuir isotherms were used to determine the adsorption

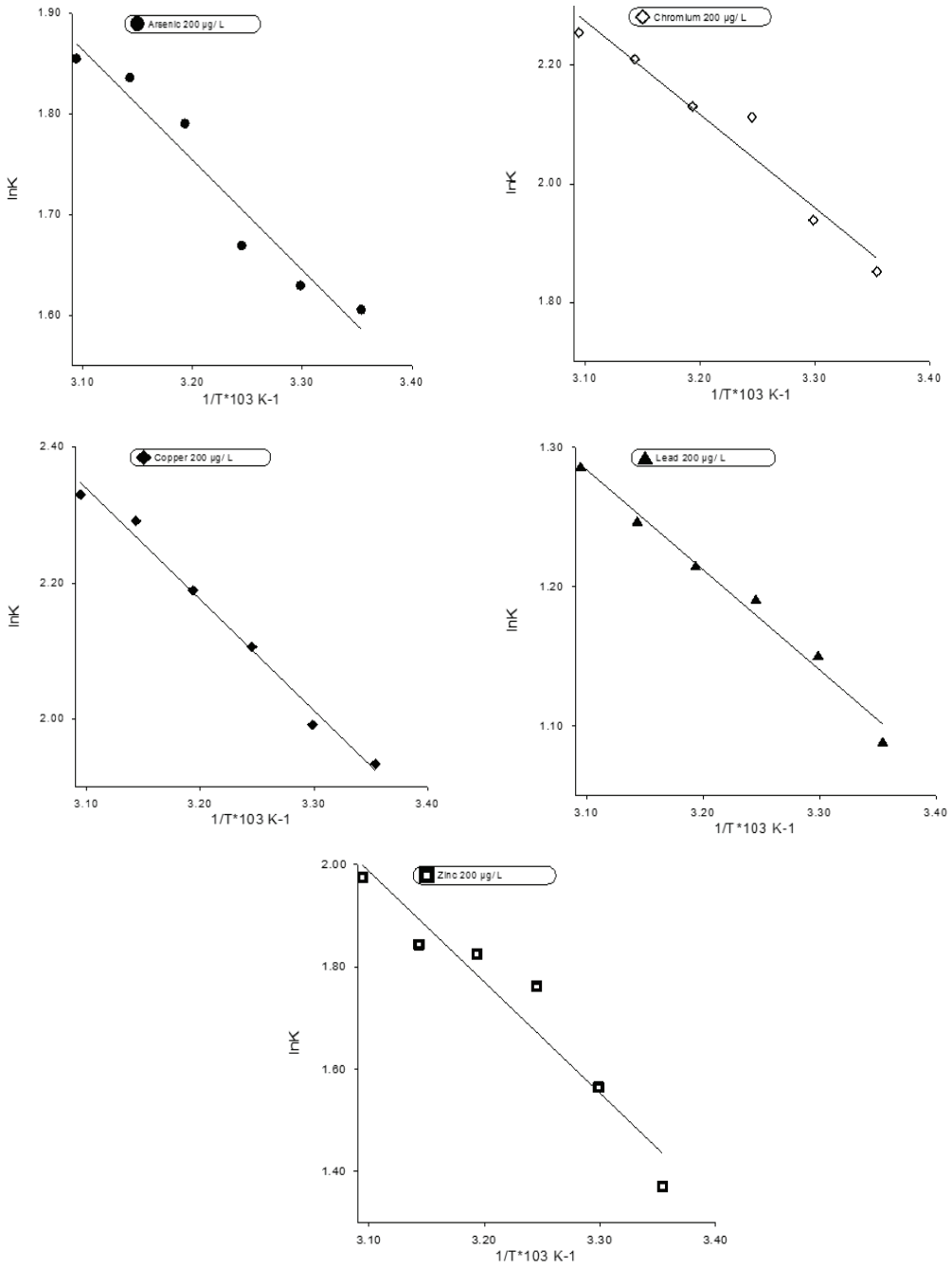

Fig. 18. Plots for Van't Hoff adsorption of metals on nanocomposite characterized from melon waste.

Table 4
Enthalpy and entropy values for the adsorption of heavy metals on carbon nanostructures prepared from melon waste

Heavy metals	$\Delta H°$	$\Delta S°$
Arsenic	–9.093	43.68
Chromium	–13.112	59.560
Copper	–13.561	61.487
Lead	–5.977	29.202
Zinc	–18.038	72.437

Table 5
Gibbs free energy $\Delta G°$ values (kJ mol^{-1}) for the adsorption of heavy metals on carbon nanostructures prepared from melon waste

Metals	Temperature (°C)					
	25	30	35	40	45	50
Arsenic	–13.03	–13.25	–13.46	–13.68	–13.90	–14.12
Chromium	–17.77	–18.06	–18.36	–18.66	–18.96	–19.25
Copper	–18.34	–18.65	–18.96	–19.26	–19.57	–19.88
Lead	–8.71	–8.85	–9.00	–9.15	–9.29	–9.44
Zinc	–21.61	–21.97	–22.33	–22.70	–23.06	–23.42

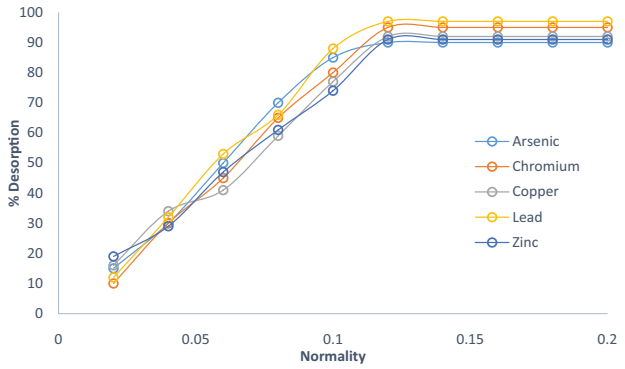

Fig. 19. Desorption of metals from the prepared adsorbent.

parameters. Other adsorption parameters like adsorption kinetics, effect of time, pH and temperature were also determined. The best fits were obtained for Freundlich isotherm and with second-order kinetic model. At high pH there was a decline in percentage adsorption. The value of $\Delta S°$ was positive while that of $\Delta H°$ and $\Delta G°$ were negative. It was concluded from data that adsorbent prepared from melon waste has high adsorption capacities and can be used as alternative of activated carbon.

References

[1] J. Chen, Analysis of water environment in the Xinjiang arid region, Arid Environ. Monit., 16 (2002) 223–227.
[2] T. Velea, L. Gherghe, V. Predica, R. Krebs, Heavy metal contamination in the vicinity of an industrial area near Bucharest, Environ. Sci. Pollut. Res., 16 (2009) S27–S32.
[3] E. Emmanuel, M.G. Pierre, Y. Perrodin, Groundwater contamination by microbiological and chemical substances released from hospital wastewater and health risk assessment for drinking water consumers, Environ. Int., 35 (2009) 718–726.
[4] S. Muhammad, M.T. Shah, S. Khan, Health risk assessment of heavy metals and their source apportionment in drinking water of Kohistan region, northern Pakistan, Microchem. J., 98 (2011) 334–343.
[5] M.M. Benjamin, K.F. Hayes, J.O. Leckic, Removal of toxic metals from power generation waste streams by adsorption and co-precipitation, J. Water Pollut. Control Fed., 54 (2002) 1472–1481.
[6] C. Namasivayam, K. Ranganathan, Removal of Cd(II) from wastewater by adsorption on waste Fe(III)/Cr(III) hydroxide, Water Res., 29 (1995) 1737–1744.
[7] D. Sud, G. Mahajan, M.P. Kaur, Agricultural waste material as potential adsorbent for sequestering heavy metal ions from aqueous solutions—a review, Bioresour. Technol., 99 (2008) 6017–6027.
[8] A. Demirbas, Heavy metal adsorption onto agro-based waste materials: a review, J. Hazard. Mater., 157 (2008) 220–229.
[9] D. Mohan, C.U. Pittman, Arsenic removal from water/wastewater using adsorbents—a critical review, J. Hazard. Mater., 142 (2007) 1–53.
[10] G. Zhang, H. Qu, R. Liu, R. Liu, R. Wu, Preparation and evaluation of a novel Fe–Mn binary oxide adsorbent for effective arsenite removal, Water Res., 41 (2007) 1921–1928.
[11] P. Mondal, C.B. Majumder, B. Mohanty, Laboratory based approaches for arsenic remediation from contaminated water: recent developments, J. Hazard. Mater., 137 (2006) 464–479.
[12] Y.B. Onundi, Y.A.A. Mamun, M.F. Al Khatib, Y.M. Ahmed, Adsorption of copper, nickel and lead ions from synthetic semiconductor industrial wastewater by palm shell activated carbon, Int. J. Environ. Sci. Technol., 7 (2010) 751–758.
[13] J. Nouri, B. Lorestani, N. Yousefi, N. Khorasani, A.H. Hasani, S. Seif, M. Cheraghi, Phytoremediation potential of native plants grown in the vicinity of Ahangaran lead–zinc mine (Hamedan, Iran), Environ. Earth Sci., 62 (2011) 639–644.
[14] G. Issabayeva, M.K. Aroua, N.M. Sulaiman, Continuous adsorption of lead ions in a column packed with palm shell activated carbon, J. Hazard. Mater., 155 (2007) 109–113.
[15] Y. B. Onundi, A.A. Mamun, Adsorption of heavy metals from synthetic industrial wastewater by activated carbon, Int. J. Environ. Sci. Technol., 7 (2012) 245–261.
[16] S.P. Singh, L.Q. Ma, M.J. Hendry, Characterization of aqueous lead removal by phosphatic clay: equilibrium and kinetic studies, J. Hazard. Mater., 136 (2006) 654–662.
[17] D.F. Samuel, M.A. Osman, Adsorption Processes for Water Treatment, Butterworths, USA, 2004.
[18] V.K. Gupta, V.K. Saini, N. Jain, Adsorption of As(III) from aqueous solutions by iron oxide-coated sand, J. Colloid Interface Sci., 288 (2005) 55–60.
[19] V. Chantawong, N.W. Harvey, V.N. Bashkin, Comparison of heavy metals adsorption by Thai kaolin and ballclay, Water Air Soil Pollut., 148 (2003) 111–125.
[20] K.P. Bong, H.S. Seung, J.Y. Young, Selective biosorption of mixed heavy metal ions using polysaccharides, Korean J. Chem. Eng., 21 (2004) 1168–1172.
[21] X. Liu, M. Kim, Solvothermal synthesis and magnetic properties of magnetite nanoplatelets, Mater. Lett., 63 (2009) 428–430.
[22] M. Sundarajan, M. Ramalakshmi, Novel cubic magnetite nanoparticle synthesis using room temperature ionic liquid, J. Chem., 9 (2012) 1070–1076.
[23] M. Zahoor, Removal of crystal violet from water by adsorbent prepared from Turkish coffee residue, Tenside Surfactants Deterg., 49 (2012) 107–113.
[24] M. Zahoor, F.A. Khan, Aflatoxin B1 detoxification by magnetic carbon nanostructures prepared from maize straw, Desal. Wat. Treat., 57 (2016) 11893–11903.
[25] L. Ai, L. Li, Efficient removal of organic dyes from aqueous solution with ecofriendly biomass-derived carbon nanocomposites by one-step hydrothermal process, Chem. Eng. J., 223 (2013) 688–695.
[26] S.A. Kahani, M. Hamadanian, O. Vandadi, Deposition of Magnetite Nanoparticles in Activated Carbons and Preparation of Magnetic Activated Carbons, 1st Sharjah International Conference on Nanotechnology and Its Applications, American Institute of Physics 978, 2007, pp. 7354–7439.

[27] C.H. Giles, T.H. Macewan, S.N. Nakhwa, D. Smith, Studies in adsorption. Part IX. A system of classification of solution adsorption isotherms and its use in diagnosis of adsorption mechanisms and in measurement of specific surface areas of solids, J. Chem. Soc., 30 (1960) 3973–3993.
[28] I. Langmuir, The adsorption of gases on plane surfaces of glass, mica and platinum, J. Am. Chem. Soc., 40 (1918) 1361–1403.
[29] H. Freundlich, Über die adsorption in lösungen (Adsorption in solution), Z. Phys. Chem., 57 (1906) 384–470.
[30] S. Lagergren, Theory of the so-called adsorption of loosened substances, K. Sven. Vetensk.akad. Handl., 24 (1898) 1–39.
[31] Y.S. Ho, G. McKay, Sorption of dye from aqueous solution by peat, Chem. Eng. J., 70 (1998) 115–124.
[32] W.J. Weber, J.C. Morris, Kinetics of adsorption on carbon from solution, J. Sanitary Eng. Div. Proc. Am. Soc. Civil Eng., 89 (1963) 31–59.